Semicond. Sci. Technol. 9 (1994) 2217–2223. Printed in the UK

Investigation of a short-period (001) $HgTe–Hg_{0.6}Cd_{0.4}Te$ superlattice by transmission electron microscopy

X F Zhang†§, C R Becker‡, H Zhang†‖, L He‡¶ and G Landwehr‡

† Institut für Festkörperforschung, Forschungszentrum Jülich GmbH, Postfach 1913, 52425 Jülich, Germany
‡ Physikalisches Institut der Universität Würzburg, Am Hubland, 97074 Würzburg, Germany

Received 11 July 1994, accepted for publication 19 September 1994

Abstract. A molecular beam epitaxially grown short-period (001) HgTe–$Hg_{0.6}Cd_{0.4}Te$ superlattice was studied by means of transmission electron microscopy and high-resolution electron microscopy (HREM). Cross sections of the as-grown samples revealed good epitaxial features and surprisingly strong contrast between HgTe and $Hg_{0.6}Cd_{0.4}Te$ layers in spite of the small difference in Cd concentration between the wells and the barriers. The fact that the variation in Cd concentration is so small is due in part to interdiffusion between the very narrow wells and barriers, which are only four and six monolayers wide, respectively. Precipitates of dimensions 1 by 12 nm have been identified in HREM images as the monoclinic, high-pressure phase of elemental Te.

1. Introduction

The HgTe–$Hg_{1-x}Cd_xTe$ superlattice (SL) was first proposed as a potential infrared material in 1979 [1] and it has received a good deal of attention over the last few years. It has been pointed out that the bandgap of this SL could be varied throughout the entire infrared spectral region by varying the thickness of the HgTe well and to a lesser extent by varying the $Hg_{1-x}Cd_xTe$ barrier thickness. Molecular beam epitaxy (MBE) or variations thereof is perhaps the best technique to prepare multilayers of this type. After the first HgTe–$Hg_{1-x}Cd_xTe$ SL was grown by means of MBE in 1982 by Faurie *et al* [2], many results on the growth and properties of this SL system have been published [3–14]. Atomic structures and, in particular, dislocations have been studied by high-resolution electron microscopy (HREM) [15]. However, there are still a number of open questions. Some of them, as stated below, are closely related to the microscopic structure of the SL, which can be investigated by transmission electron microscopy (TEM).

Intermixing of the HgTe and $Hg_{1-x}Cd_xTe$ layers has attracted much attention because this would cause a change in the composition of the wells and barriers, and consequently would affect the properties of this SL system such as the bandgap, as proposed by Schulman and Chang [16]. In spite of many previous diffusion investigations [3, 4, 7, 17–20] knowledge of the microscopic structure of the diffused HgTe–$Hg_{1-x}Cd_xTe$ SL is not complete and the results in the literature are not always consistent.

Defects such as precipitates and dislocations in $Hg_{1-x}Cd_xTe$ and CdTe have been the subject of numerous investigations [15, 21–26], but to our knowledge no HREM results on precipitates with atomic resolution have been published. Therefore an investigation of precipitates with atomic resolution was undertaken. In addition, misfit dislocations could be present in the SL in order to accommodate the strain fields caused by the lattice mismatch between heterolayers. Furthermore, knowledge of the crystal structure and composition in the vicinity of the film–substrate interface is also very important in improving the quality of the SL films.

It is of interest to note that most of the published work to date on the HgTe–$Hg_{1-x}Cd_xTe$ SL is concentrated on superlattices whose periods are

§ On leave from Beijing Laboratory of Electron Microscopy, Chinese Academy of Sciences, PO Box 2724, Beijing 100080, People's Republic of China.

‖ Present address: Materials Science and Technology Park, Northwestern University, 2225 Sheridan Road, Evanston, IL 60208, USA.

¶ Permanent address: Shanghai Institute of Technical Physics, Chinese Academy of Sciences, Shanghai, People's Republic of China.

0268-1242/94/122217+07$19.50

appreciably larger than 3 nm. In this article, we report on TEM studies of an MBE-grown (001) HgTe–$Hg_{1-x}Cd_xTe$ SL with the extremely short period of 3.2 nm.

2. Experimental details

Four (001) HgTe–$Hg_{1-x}Cd_xTe$ superlattices with 900 periods were grown simultaneously by MBE on (001) $Cd_{0.96}Zn_{0.04}Te$ substrates. Epitaxial growth was carried out in a four-chamber RIBER 2300 MBE system. The substrates were degreased, chemo-mechanically polished and etched as has been described previously [27]. A thin CdTe buffer of about 30 nm was grown at 270 °C and the SL was grown at 180 °C. The thickness of the HgTe well is 1.1 nm and that of the $Hg_{1-x}Cd_xTe$ barrier is 2.0 nm, as determined directly with a five-crystal x-ray diffractometer [27, 28], i.e. the period is 3.14 nm. Details of the corresponding x-ray analyses of this SL and its growth have been published elsewhere [27]. The substrate temperature was measured with an accuracy of ±2 °C by means of a thermocouple which was in physical contact with the molybdenum substrate holder. The thermocouple was carefully calibrated at the melting point of indium.

In order to prepare the cross-section samples for TEM examination, an as-grown sample was cut into small square pieces with {110}-type edges. The small pieces were then glued face to face with epoxy resin and thinned so as to ensure transparency to electrons first by mechanical methods and thereafter by means of Ar ion milling on a liquid-nitrogen-cooled stage. TEM experiments were performed in a JEOL 4000EX transmission electron microscope operated at 400 kV.

3. Results

The morphology of a cross section is shown in figure 1. The buffer layer between the SL and the substrate is 30 to 40 nm thick and is indicated by BF in figure 1. An ambiguous interface is visible between the substrate and the buffer while, as may be expected, a sharp and smooth interface is present between the SL and the buffer. The latter interface is indicated by a pair of arrows.

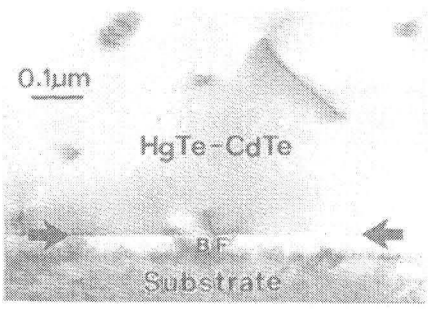

Figure 1. The morphology of a superlattice–substrate region. The interface between the superlattice and the buffer is indicated by a pair of arrows. The position of the buffer is shown by the letters BF.

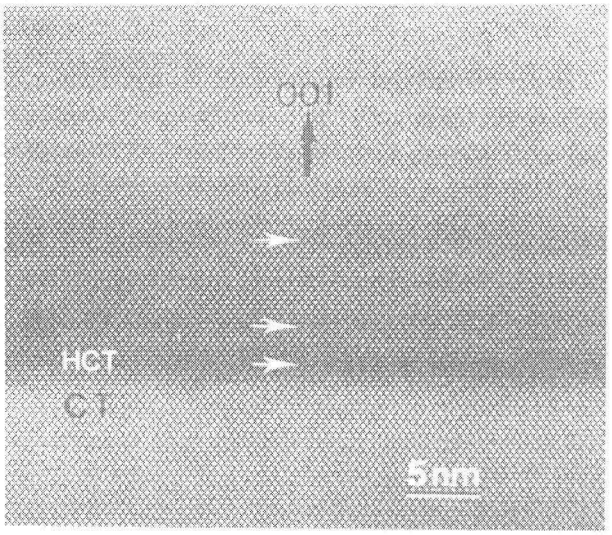

Figure 2. A micrograph of the SL–buffer interface region. HCT and CT denote the first $Hg_{1-x}Cd_xTe$ layer of the superlattice and the CdTe buffer respectively. Three relatively thick $Hg_{1-x}Cd_xTe$ layers are indicated by white arrows.

Figure 2 is a micrograph which shows a region close to the SL–buffer interface. This interface can be readily recognized by comparing the alternately stacked darker and brighter layer structure of the SL with the homogeneous brightness of the buffer. From the deposition sequence, the darker and brighter layers are known to be $Hg_{1-x}Cd_xTe$ and HgTe respectively. The quality of the very first layers of the SL is good in spite of the somewhat irregular thicknesses of these $Hg_{1-x}Cd_xTe$ and HgTe layers. Moreover, after the first five periods the thicknesses of these HgTe and $Hg_{1-x}Cd_xTe$ layers are constant within experimental errror. No misfit dislocations or specific structural defects were resolved in the vicinity of the SL–buffer interface.

A $[1\bar{1}0]$ bright-field image and a corresponding selected-area electron diffraction pattern are shown in figures 3(*a*) and (*b*) respectively. Somewhat irregular interfaces between HgTe and $Hg_{1-x}Cd_xTe$ layers can be seen and a defect is indicated by a bold arrow. The period of the SL in the region displayed in figure 3(*a*) is 3.3 nm. This was confirmed by means of the electron diffraction pattern shown in figure 3(*b*). The main reflections arising from HgTe and $Hg_{1-x}Cd_xTe$ coincide because of the extremely small difference between their lattice parameters: the lattice parameter for HgTe is 0.6461 nm and that for CdTe is 0.6482 nm [29]. The first- and second-order satellites, which are due to the periodicity of the superlattice, are indicated by black arrowheads and a white arrow respectively. These satellites fall along the [001] direction of the main reflections and correspond to a superlattice period of about 3.4 nm along the [001] direction in real space. This value is consistent with the 3.3 nm obtained from figure 3(*a*), within the experimental error of about 10%.

Figure 4 is a HREM image taken along the $[1\bar{1}0]$ direction of the $Hg_{1-x}Cd_xTe$ structure. This HREM image was obtained with an acceleration voltage of 400 kV, a spherical aberration (Cs) of 1 mm, a Sherzer

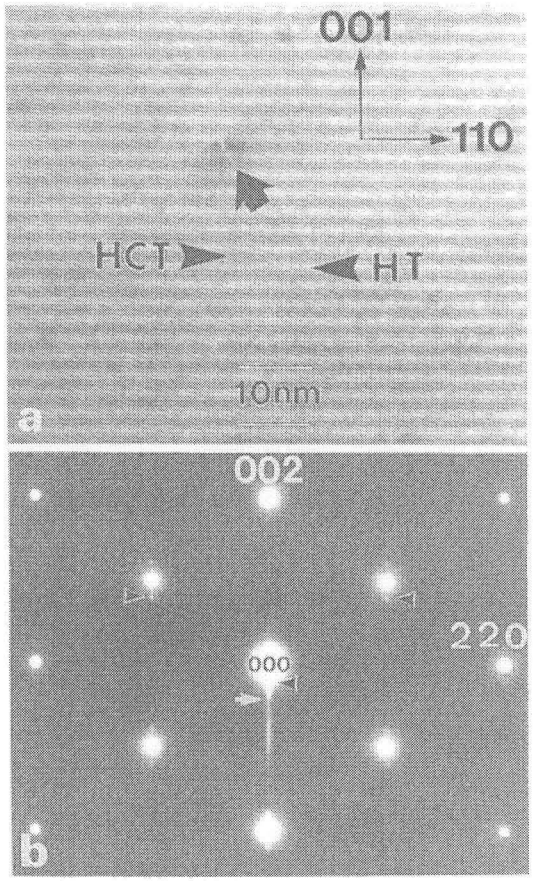

Figure 3. (*a*) A bright-field fringe image taken along the [110] direction of the $Hg_{1-x}Cd_xTe$ structure. HT and HCT represent HgTe and $Hg_{1-x}Cd_xTe$ respectively. A defect is indicated by the bold arrow. (*b*) A $(1\bar{1}0)$ electron diffraction pattern. Basic reflections are indexed according to the $Hg_{1-x}Cd_xTe$ zinc blende structure. The first- and second-order satellites along the [001] direction are indicated by black arrowheads and a white arrow respectively.

defocus of −40 to −50 nm, a defocus spread of 10 nm and an illumination half-angle of 1.0 mrad. The brighter HgTe layers and the darker $Hg_{1-x}Cd_xTe$ layers can be better distinguished along the [110] direction (horizontal) by viewing from the side at a glancing angle. Close inspection of this local region shows that an average period consists of four HgTe monolayers (brighter) and six $Hg_{1-x}Cd_xTe$ monolayers (darker) along the [001] direction. Thus the average thicknesses of the HgTe and $Hg_{1-x}Cd_xTe$ layers are 1.3 and 1.9 nm respectively, and the period is 3.2 nm in agreement with that concluded from figure 3. The average thicknesses of the wells and the barriers according to x-ray diffraction, 1.1 and 2.0 nm, corroborate the HREM results.

The {111}-type lattice fringes in figure 4 run across the interfaces between HgTe and $Hg_{1-x}Cd_xTe$ layers without any major disturbance, albeit with appreciable waviness which may be due to interdiffusion between the layers.

In order to test the feasibility of the imaging conditions necessary for the observed contrast in HgTe–$Hg_{1-x}Cd_xTe$ heterostructures, image simulations were carried out for x values of 1, 0.4, 0.3 and 0.2 by means of the EMS computer code [30], assuming no lattice

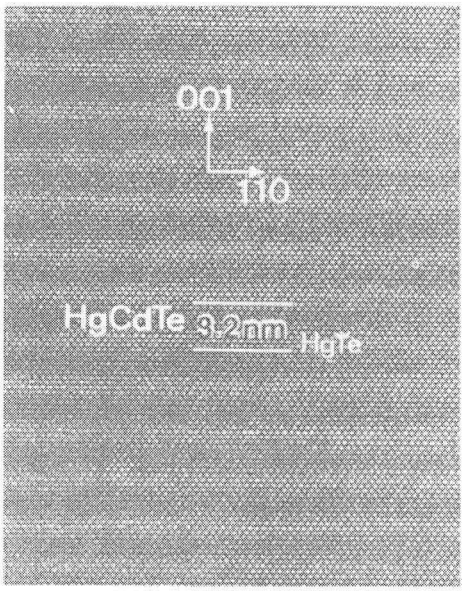

Figure 4. An HREM image viewed along the $[1\bar{1}0]$ direction. The period of the superlattice is marked by a pair of lines.

distortions. Our computer simulations suggest that there should be no discernible contrast between HgTe and CdTe layers when the defocus of the objective lens is changed from −30 to −70 nm if the crystal thickness is less than 11 nm or more than 16 nm. However, an observable image contrast between HgTe and CdTe can be achieved under the conditions of a −40 or −50 nm defocus together with a crystal thickness of about 14.4 ± 2 nm (the Scherzer defocus of the JEOL 4000EX electron microscope is about −50 nm). Under these imaging conditions, the HgTe layers are brighter than the CdTe layers. In addition, the simulations predict a weaker but observable contrast between HgTe and $Hg_{1-x}Cd_xTe$ for these imaging conditions when $0.3 \leqslant x \leqslant 1$. Even though the resulting contrast for $x = 0.4$ fits that of the experimental observations in figure 4 reasonably well, the perception of this contrast is difficult due to the extremely high resolution of the simulation. Hence, for demonstration purposes, the simulation of HgTe and CdTe layers is shown in figure 5. The reduction or even the disappearance of the contrast between HgTe and $Hg_{1-x}Cd_xTe$ in some regions can be attributed to these fairly strict imaging conditions.

A defect region near the SL–buffer interface is shown in figure 6(*a*). A defect can be seen about 20 nm above the buffer surface. An image of this defect with a higher magnification is shown in figure 6(*b*). This defect can be thought of as a small mosaic crystalline slab whose extended plane is parallel to the (110) plane of the $Hg_{1-x}Cd_xTe$ matrix. Its size is about 12 nm in the (110) plane and 0.9 nm along a direction perpendicular to the (110) plane. A spherically symmetric strain field with a diameter of about 12 nm is apparent from the contrast variation in this region. The lattice match between this slab and the $Hg_{1-x}Cd_xTe$ matrix is good along (001) and (110) atomic planes but stacking faults are present along

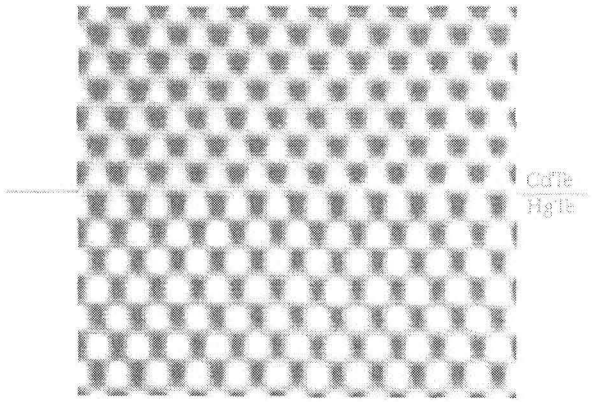

Figure 5. Image simulations of a HgTe–CdTe interface for a sample thickness of 14.4 nm and a defocus of −50 nm.

{111} planes of the $Hg_{1-x}Cd_xTe$.

A different lattice arrangement can be distinguished inside the slab, which lies between a pair of arrows in figure 6(*b*). Details can be clearly seen in figure 7, which shows part of the region in figure 6(*b*) at a higher magnification. The part of the image indicated by a pair of arrows in figure 7 was processed by means of a computer program for digital image processing and the results are shown in the inset (*a*) in figure 7. The large bright dots in figure 7 correspond to the $Hg_{1-x}Cd_xTe$ matrix while the small bright dots correspond to the mosaic crystal.

In order to characterize the structure and composition of this small crystalline slab, computer simulations were performed using the program described above [30]. Pure Hg could be excluded after a series of calculations with various values for the defocus and crystal thicknesses as well as for different zone-axis directions. Pure Cd is not stable and is also unlikely according to the image simulation. However, good agreement can be achieved with a simulation of monoclinic Te, whose lattice parameters [31] are $a = 0.3104$ nm, $b = 0.7513$ nm, $c = 0.4766$ nm and $\beta = 92.71°$, but not with hexagonal Te. The [010] direction of the monoclinic Te is parallel to [1$\bar{1}$0] of the $Hg_{1-x}Cd_xTe$

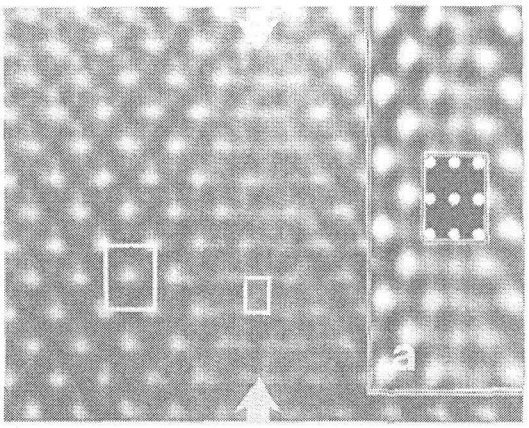

Figure 7. A magnification of part of the defect region in figure 6. The defect is indicated by a pair of white arrows. The inset (*a*) is an enlargement of the corresponding computer-processed image of the defect. A computer-simulated image of the Te structure is shown in the small rectangle in this inset. This rectangle corresponds to the smaller rectangle between the two white arrows.

matrix, i.e. perpendicular to the image plane. The values of the parameters used in this simulation are the same as the experimental values listed above, which include a defocus of −50 nm together with a crystal thickness of about 6 nm. The resulting computer-simulated image is shown in the small rectangle in the centre of inset (*a*) in figure 7. According to the previous computer simulation mentioned above, the SL thickness necessary for the near absence of contrast between the HgTe and $Hg_{1-x}Cd_xTe$ layers (< 12 nm or > 17 nm) shown in figure 6 is consistent with the 6 nm thickness used in this computer simulation of monoclinic Te. Te precipitates can be caused by inappropriate local growth parameters [32]. Te-rich compounds that have nearly the same structure as that of pure Te are also possible. In addition to these defects, dislocations have also been observed in our $Hg_{1-x}Cd_xTe$ films.

Small circular or elliptical loops are displayed in figure 8. Some are indicated by arrowheads. The size of these loops varies between 10 and 50 nm. The corresponding reciprocal vectors g_1 and g_2 of the

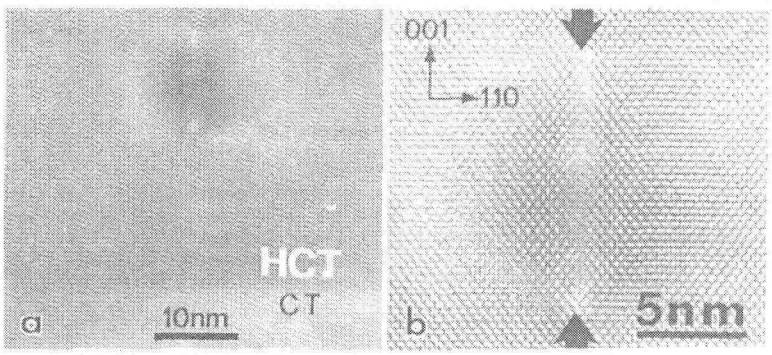

Figure 6. (*a*) Micrograph showing a mosaic crystal in the SL. HCT and CT represent the first $Hg_{1-x}Cd_xTe$ layer of the superlattice and the CdTe buffer respectively. The defect region is seen at a lower magnification in (*a*) and a higher magnification in (*b*). A pair of bold arrows in (*b*) defines this defect region, which has a lattice constant different from that of the $Hg_{1-x}Cd_xTe$ matrix.

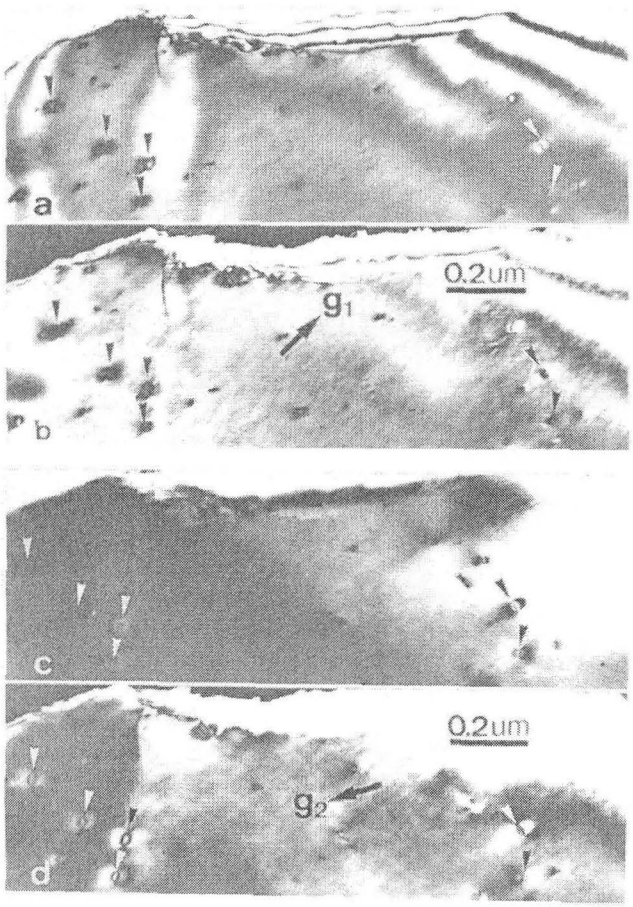

Figure 8. (*a*) and (*b*) are a pair of bright- and dark-field diffraction contrast images and $g_1 = [111]$ is the corresponding reciprocal vector of the electrons used to make these images. (*c*) and (*d*) are a pair of bright- and dark-field diffraction contrast images of the same region shown in (*a*) and (*b*) but with a different reciprocal vector for the electrons, $g_2 = [331]$. Some dislocation loops are indicated by arrowheads. No loops have been found with contrast-free lines that are simultaneously perpendicular to both g_1 in (*a*) and (*b*), and g_2 in (*c*) and (*d*). Note that the dislocation loops indicated in (*a*) and (*b*) have different shapes in (*c*) and (*d*).

electron beam used to make these images are indicated in the dark-field diffraction contrast images shown in figures 8(*b*) and (*d*) respectively, where $g_1 = [111]$ and $g_2 = [331]$. The reciprocal vector was changed merely by tilting the sample. No loops with contrast-free lines perpendicular to g_1 in figures 8(*a*) and (*b*) and simultaneously perpendicular to g_2 in figures 8(*c*) and (*d*) have been found. This implies that they are dislocation loops rather than being caused by precipitates. Furthermore, the loops indicated by arrowheads in figures 8(*a*) and (*b*) have different shapes to those in figures 8(*c*) and (*d*) (note the variation of the central region for each loop indicated). This excludes the possibility that precipitates with a spherically symmetric strain field have caused these loops because these precipitates will, in principle, have similar shapes when viewed along different zone-axis directions. Cullis *et al* [33] have demonstrated that dislocation loops can be caused in CdTe during sample preparation by Ar ion milling. Hence some or all of these dislocation loops may be due to Ar ion bombardment. The electron beam used for HREM images may possibly damage the sample, but no apparent damage occurred within the first few tens of seconds, which is enough time to yield good quality HREM images.

4. Discussion

4.1. Te precipitates

Te precipitates have been observed and studied in detail in bulk $Hg_{1-x}Cd_xTe$ [22] and in both bulk and MBE-grown CdTe [21, 23]. Schaake *et al* [22] found both the trigonal and the monoclinic phases, i.e. low and high pressure phases, in solid state recrystallized $Hg_{1-x}Cd_xTe$. Furthermore they have shown that these precipitates nucleate at dislocations as well as in a matrix on impurities or homogeneously. The size of the former precipitates is of the order of 0.1 μm and that of the latter is less than 40 nm. Shin *et al* [21] identified only the high pressure phase in bulk CdTe whereas Chew *et al* [23] observed the low pressure phase in MBE-grown CdTe. However, the precipitates observed by Chew *et al* were in polycrystalline CdTe grown at a lower temperature than normal. These precipitates are also quite large, i.e. 0.1 μm and larger. The precipitates that have been observed in this investigation are extremely small, approximately 0.9 by 12 nm, and are the high pressure phase of Te. In the light of the above, apparently small monoclinic Te precipitates occur if growth conditions are close to ideal and the system nearly stoichiometric. Conversely, large trigonal Te precipitates result if conditions are appreciably less than ideal, i.e. during quenching or polycrystalline growth.

4.2. Interdiffusion between HgTe and $Hg_{1-x}Cd_xTe$

The number of satellites in a diffraction experiment is a good criterion for the structural quality of a superlattice only if the width of the interfaces is small compared with the period. As shown in figures 3(*a*) and 4, the HgTe–$Hg_{1-x}Cd_xTe$ interface is not abrupt. This lack of abruptness is caused by the randomness inherent in the $Hg_{1-x}Cd_xTe$ alloy in the barrier and subsequent diffusion between the barriers and wells during growth at the temperature of 180 °C. This interface width can be used to explain the presence of only two orders of satellites in the corresponding electron diffraction pattern in figure 3(*b*); the number of observed satellites is a rough qualitative measure of the interfacial abruptness of heterojunctions. The corresponding (004) x-ray rocking curve also has only first- and second-order satellites, but computer simulations of the satellite intensities are in good agreement with the experimental x-ray intensities [27]. For example, this is true if the experimentally determined Cd concentration profile across the HgTe–$Hg_{1-x}Cd_xTe$ interface according to Kim *et al* [19] is employed. This interface is about three to four

monolayers wide. If the interface is assumed to be abrupt then the satellite intensities are one or two orders of magnitude too large. Furthermore, if an interface with twice the above width is used then the second-order satellites disappear. Superlattices with larger periods that have been grown under the same experimental conditions have up to seventh-order satellites in their (004) rocking curves [27].

As is normally the case, these HgTe–$Hg_{1-x}Cd_xTe$ superlattices were grown with a constant Hg flux. Barrier material grown under the prevailing conditions has an x value of 0.70. An upper limit on the average Cd concentration of the barriers themselves was established by annealing one of the superlattices in Hg vapour, pressure 80 Torr, at 250 °C for 24 hours [27]. The Cd concentration of the resulting $Hg_{1-x}Cd_xTe$ alloy was determined from the E_0 bandgap to be 23.0 at.%. This means that the average Cd concentration, $\bar{x}_b$, in the barriers is 36 at.% if no Cd is present in the wells. For these narrow wells this does not seem to be a good assumption. Therefore $\bar{x}_b = 0.36$ is an upper limit for this superlattice. For example, if $\bar{x}_w = 0.05$ then $\bar{x}_b = 0.33$. These results are to a good approximation consistent with the maximum value in the barrier of 0.4, which is necessary to calculate the correct optical absorption coefficient [34].

It is somewhat surprising that interdiffusion has not totally obscured these interfaces. Kim *et al* [19] found that interdiffusion is a sensitive function of the distance from the sample surface, i.e. interdiffusion is two orders of magnitude less at an interface depth of 700 nm than at 10 nm. Their published values for the Hg diffusion constant at 180 °C are approximately 1×10^{-17}, 1×10^{-18} and 1×10^{-19} $cm^2 s^{-1}$ for depths of 10, 350 and 700 nm respectively. The interfaces observed in our investigation are all close to the buffer and thus far from the surface of the superlattice, which is 2.84 μm thick. The time spent during growth at a distance of 350 nm or less from the surface was 30 minutes. Therefore, in spite of the growth time of nearly 4 hours at 180 °C the values for the diffusion constant according to Kim *et al* are consistent with the fact that the HgTe–$Hg_{0.6}Cd_{0.4}Te$ interfaces have not been completely obliterated, i.e. $2\pi\sqrt{Dt} \approx 2$ nm where D is the diffusion constant at a depth of 350 nm and t is the time.

Large variations in the $Hg_{1-x}Cd_xTe$ layer thickness are apparent in the region near the SL–buffer interface as indicated by white arrows in figure 2. These layers have a thickness of about 2.5 nm rather than the average thickness of 1.9 nm. Since this variation occurred only within 15 nm of the buffer, it can be regarded as due to a deviation of the initial fluxes from their later steady-state values.

4.3. HgTe–$Hg_{1-x}Cd_xTe$ and SL–buffer interfaces

In general, a periodic arrangement of misfit dislocations occurs at the interface of heterostructures to accommodate the strain relaxtion caused by the lattice mismatch. However, in our samples, the lattice mismatches between HgTe and $Hg_{0.6}Cd_{0.4}Te$ and between the SL and the $Cd_{0.96}Zn_{0.04}Te$ substrate are only 0.1 and 0.02% respectively. In addition, the formation of misfit dislocations at the SL–buffer interface is also hindered by the low substrate temperature (180 °C) used during the MBE growth. The thermal expansion coefficients of HgTe and $Hg_{1-x}Cd_xTe$ differ only slightly, i.e. 4.0×10^{-6}/°C for HgTe, 4.9×10^{-6}/°C for CdTe and an intermediate value for $Hg_{1-x}Cd_xTe$ [35].

Therefore, the resulting small strain fields and the very thin layers can be expected to induce only a small number of misfit dislocations. According to our HREM observations, no misfit dislocations were identified in either the HgTe–$Hg_{1-x}Cd_xTe$ interfaces or the SL–buffer interface, as shown for example in figure 2. It should be pointed out that this statement implies only an upper limit for the misfit dislocation density of approximately 10^9 to 10^{10} cm^{-2} due to the very nature of HREM investigations, i.e. the relatively low number of observations. Dislocations can be more easily observed in bright-field and dark-field images, as for example in figure 1, but the dislocation type cannot be determined without elaborate analysis. Chami *et al* [25] have shown that channelling is a more appropriate method to determine the low misfit dislocation densities that occur in nearly lattice-matched heterostructures.

Consequently, the relatively good quality of the superlattices investigated can be partly attributed to the generation of only a few misfit dislocations [32]. It should be pointed out that the CdTe buffer may play an important role in improving the quality of the films. This can be concluded from figure 1, in which a rather disordered buffer–substrate is followed by a much smoother and sharper SL–buffer interface.

5. Conclusion

An extremely short-period MBE-grown (001) HgTe–$Hg_{0.6}Cd_{0.4}Te$ superlattice on a $Cd_{0.96}Zn_{0.04}Te$ substrate was studied by TEM. The superlattice was found to have a constant period after the initial five or so periods. The average layer thicknesses for the HgTe and $Hg_{1-x}Cd_xTe$ layers, which were determined to be four and six monolayers wide respectively, were corroborated by x-ray diffraction measurements. Interdiffusion of the HgTe and the $Hg_{1-x}Cd_xTe$ layers is consistent with the published diffusion constant for Hg [19]. Some nanometre-size defects, such as Te precipitates with a nearly spherically symmetric strain field, as well as dislocations and dislocation loops were observed. These precipitates have been shown to be the monoclinic, high-pressure phase of Te.

Acknowledgments

The support of this investigation by the Bundesministerium für Forschung und Technologie in Bonn, contract number TK 0369, and the Alexander von Humboldt Stiftung is gratefully acknowledged.

References

[1] Schulman J N and McGill T C 1979 *Appl. Phys. Lett.* **34** 663

[2] Faurie J P, Million A and Piaguet J 1982 *Appl. Phys. Lett.* **41** 713

[3] Harris K A, Hwang S, Blanks D K, Cook J W Jr, Schetzina J F, Otsuka N, Baukus J P and Hunter A T 1986 *Appl. Phys. Lett.* **48** 396

[4] Faurie J P, Sivananthan S and Reno J 1986 *J. Vac. Sci. Technol.* A **4** 2096

[5] Harris K A, Hwang S, Blanks D K, Cook J W Jr, Schetzina J F and Otsuka N 1986 *J. Vac. Sci. Technol.* A **4** 2061

[6] Arch D K, Staudenmann J L and Faurie J P 1986 *Appl. Phys. Lett.* **48** 1588

[7] Perkowitz S, Rajavel D, Sou I K, Reno J, Faurie J P, Jones C E, Casselman T, Harris K A, Cook J W Jr and Schetzina J F 1986 *Appl. Phys. Lett.* **49** 806

[8] Harris K A, Hwang S, Lansari Y, Cook J W Jr, Schetzina J F and Otsuka N 1986 *Appl. Phys. Lett.* **49** 713

[9] Hoffman C A, Meyer J R, Youngdale E R, Lindle J R, Bortoli F J, Han J W, Harris K A, Cook J W Jr and Schetzina J F 1988 *J. Vac. Sci. Technol.* A **6** 2785

[10] Lansari Y, Han J W, Hwang S, Kim L S, Cook J W Jr, Schetzina J F, Schulman J N and Otsuka N 1989 *J. Vac. Sci. Technol.* B **7** 241

[11] Sporken R, Sivananthan S, Faurie J P, Ehlers D H, Fraxedas J, Ley L, Pireaux J J and Caudano R 1989 *J. Vac. Sci. Technol.* A **7** 427

[12] Mahavadi K K, Bleuse J, Chu X and Faurie J P 1989 *Appl. Phys. Lett.* **55** 1285

[13] Cesar C L, Islam M N, Feldman R D, Austin R F, Chemla D S, West L C and DiGiovanni A E 1990 *Appl. Phys. Lett.* **56** 283

[14] Mahavadi K K, Sivananthan S, Lange M D, Chu X, Bleuse J and Faurie J P 1990 *J. Vac. Sci. Technol.* A **8** 1210

[15] Di Cioccio L, Hewat E A, Million A, Gailliard J P and Dupuy M 1987 *Semiconductor Materials Conf., Oxford, 6–8 April*

[16] Schulman J N and Chang Y C 1985 *Appl. Phys. Lett.* **46** 571

[17] Cirlin E H, Ireland P, Buckingham S and Wu O 1988 *J. Vac. Sci. Technol.* A **6** 2631

[18] Otsuka N, Ihm Y E, Harris K A, Cook J W Jr and Schetzina J F 1987 *J. Vac. Sci. Technol.* A **5** 3129

[19] Kim Y, Ourmazd A, Bode M and Feldman R D 1989 *Phys. Rev. Lett.* **63** 636

[20] Tardot A, Hamoudi A, Magnea N, Gentile P and Pautrat J L 1993 *Semicond. Sci. Technol.* **8** S276

[21] Shin S H, Bajaj J, Moudy L A and Cheung D T 1983 *Appl. Phys. Lett.* **43** 68

[22] Schaake H F, Tregilgas J H, Lewis A J and Everett P M *1983 J. Vac. Sci. Technol.* A **1** 1625

[23] Chew N G, Cullis A G and Williams G M 1984 *Appl. Phys. Lett.* **45** 1090

[24] Sporken R, Sivananthan S, Reno J and Faurie J P 1988 *J. Vac. Sci. Technol.* B **6** 1204

[25] Chami A C, Ligeon E, Danielou R, Fontenille J, Lentz G, Magnea N and Mariette H 1988 *Appl. Phys. Lett.* **52** 1874

[26] Takigawa H, Yoshikawa M and Maekawa T 1988 *J. Crystal Growth* **86** 446

[27] Becker C R, He L, Regnet M M, Kraus M M, Wu Y S, Landwehr G, Zhang X F and Zhang H 1993 *J. Appl. Phys.* **74** 2486

[28] Kraus M M, Regnet M M, Becker C R, Bicknell-Tasssius R N and Landwehr G 1992 *J. Appl. Phys.* **71** 5610

[29] Regnet M M private communication

[30] Stadelmann P A 1987 *Ultramicroscopy* **21** 131

[31] Villars and Calvert L D *Pearson's Handbook of Crystallographic Data for Intermetallic Phases* vol 1 (Metals Park, OH: American Society for Metals)

[32] Li J, He L, Zhu N, Lao P and Yuan S 1992 *J. Crystal Growth* **119** 322

[33] Cullis A G and Chew N G 1985 *Ultramicroscopy* **17** 203

[34] Becker C R, Latussek V, Heinke H, Regnet M M, Goschenhofer F, Einfeldt S, He L, Bangert E and Landwehr G 1993 *Proc. SPIE Conf. on the Growth and Characterization of Materials for Infrared Detectors* **2021** 138

[35] 1982 *Landolt-Börnstein, New Series* vol 17/b *Semiconductors: Physics of II–VI and I–VII Compounds, Semimagnetic Semiconductors* ed O Madelung *et al* (Berlin: Springer)